COMPUTING GROUND STATES OF SPIN-1 BOSE-EINSTEIN CONDENSATES BY THE NORMALIZED GRADIENT FLOW

WEIZHU BAO * AND FONG YIN LIM †

Abstract. In this paper, we propose an efficient and accurate numerical method for computing the ground state of spin-1 Bose-Einstein condensates (BEC) by using the normalized gradient flow or imaginary time method. The key idea is to find a third projection or normalization condition based on the relation between the chemical potentials so that the three projection parameters used in the projection step of the normalized gradient flow are uniquely determined by this condition as well as the other two physical conditions given by the conservation of total mass and total magnetization. This allows us to successfully extend the most popular and powerful normalized gradient flow or imaginary time method for computing the ground state of single component BEC to compute the ground state of spin-1 BEC. An efficient and accurate discretization scheme, the backward-forward Euler sine-pseudospectral method (BFSP), is proposed to discretize the normalized gradient flow. Extensive numerical results on ground states of spin-1 BEC with ferromagnetic/antiferromagnetic interaction and harmonic/optical lattice potential in one/three dimensions are reported to demonstrate the efficiency of our new numerical method.

Key words. Spin-1 Bose-Einstein condensate, coupled Gross-Pitaevskii equations, ground state, normalized gradient flow, backward-forward Euler sine-pseudospectral method

AMS subject classifications. 35Q55, 65T99, 65Z05, 65N12, 65N35, 81-08

1. Introduction.

Research in low temperature dilute atomic quantum gases remains active for more than ten years after the experimental realizations of Bose-Einstein condensation (BEC) in alkali atomic gases in 1995 [2, 12, 17]. Extensive theoretical and experimental studies have been carried out to investigate various novel phenomena of the condensates. In earlier BEC experiments, the atoms were confined in magnetic trap [2, 12, 17], in which the spin degrees of freedom is frozen. The particles are described by a scalar model and the wavefunction of the particles is governed by the Gross-Pitaevskii equation (GPE) within the mean-field approximation [16, 11, 23]. In recent years, experimental achievement of spin-1 and spin-2 condensates [10, 18, 21, 26, 28] offers new regimes to study various quantum phenomena that are generally absent in a single component condensate. The spinor condensate is achieved experimentally when an optical trap, instead of a magnetic trap, is used to provide equal confinement for all hyperfine states.

The theoretical studies of spinor condensate have been carried out in several papers since the achievement of it in experiments [19, 20, 22, 27]. In contrast to single component condensate, a spin-F ($F \in \mathbb{N}$) condensate is described by a generalized coupled GPEs which consists of $2F+1$ equations, each governing one of the $2F+1$ hyperfine states ($m_F = -F, -F+1, ..., F-1, F$) within the mean-field approximation. For a spin-1 condensate, at temperature much lower than the critical temperature T_c, the three-components wavefunction $\Psi(\mathbf{x}, t) = (\psi_1(\mathbf{x}, t), \psi_0(\mathbf{x}, t), \psi_{-1}(\mathbf{x}, t)^T$ are well

*Department of Mathematics and Center for Computational Science and Engineering, National University of Singapore, Singapore 117543 (*bao@math.nus.edu.sg*, URL: http://www.math.nus.edu.sg/~bao/)

†Department of Mathematics and Center for Computational Science and Engineering, National University of Singapore, Singapore 117543 (*fongyin.lim@nus.edu.sg*).

described by the following coupled GPEs [27, 29, 30, 31],

$$i\hbar\,\partial_t\psi_1(\mathbf{x},t) = \left[-\frac{\hbar^2}{2m}\nabla^2 + V(\mathbf{x}) + (c_0+c_2)\left(|\psi_1|^2+|\psi_0|^2\right) + (c_0-c_2)|\psi_{-1}|^2\right]\psi_1$$
$$+c_2\,\bar{\psi}_{-1}\,\psi_0^2, \tag{1.1}$$
$$i\hbar\,\partial_t\psi_0(\mathbf{x},t) = \left[-\frac{\hbar^2}{2m}\nabla^2 + V(\mathbf{x}) + (c_0+c_2)\left(|\psi_1|^2+|\psi_{-1}|^2\right) + c_0|\psi_0|^2\right]\psi_0$$
$$+2c_2\,\psi_{-1}\,\bar{\psi}_0\,\psi_1, \tag{1.2}$$
$$i\hbar\,\partial_t\psi_{-1}(\mathbf{x},t) = \left[-\frac{\hbar^2}{2m}\nabla^2 + V(\mathbf{x}) + (c_0+c_2)\left(|\psi_{-1}|^2+|\psi_0|^2\right) + (c_0-c_2)|\psi_1|^2\right]\psi_{-1}$$
$$+c_2\,\psi_0^2\,\bar{\psi}_1. \tag{1.3}$$

Here, $\mathbf{x} = (x,y,z)^T$ is the Cartesian coordinate vector, t is time, $\hbar$ is the Planck constant, m is the atomic mass, and $V(\mathbf{x})$ is the external trapping potential. When a harmonic trap potential is considered,

$$V(\mathbf{x}) = \frac{m}{2}(\omega_x^2x^2 + \omega_y^2y^2 + \omega_z^2z^2), \tag{1.4}$$

with ω_x, ω_y and ω_z being the trap frequencies in the x-, y- and z-direction, respectively. $\bar{f}$ and $\mathrm{Re}(f)$ denote the conjugate and real part of the function f, respectively. There are two atomic collision terms, $c_0 = \frac{4\pi\hbar^2}{3m}(a_0+2a_2)$ and $c_2 = \frac{4\pi\hbar^2}{3m}(a_2-a_0)$, expressed in terms of the s-wave scattering lengths, a_0 and a_2, for scattering channel of total hyperfine spin 0 (anti-parallel spin collision) and spin 2 (parallel spin collision), respectively. The usual mean-field interaction, c_0, is positive for repulsive interaction and negative for attractive interaction. The spin-exchange interaction, c_2, is positive for antiferromagnetic interaction and negative for ferromagnetic interaction. The wave function is normalized according to

$$\|\Psi\|^2 := \int_{\mathbb{R}^3}|\Psi(\mathbf{x},t)|^2\,d\mathbf{x} = \int_{\mathbb{R}^3}\sum_{l=-1}^{1}|\psi_l(\mathbf{x},t)|^2\,d\mathbf{x} := \sum_{l=-1}^{1}\|\psi_l\|^2 = N, \tag{1.5}$$

where N is the total number of particles in the condensate.

By introducing the dimensionless variables: $t \to t/\omega_m$ with $\omega_m = \min\{\omega_x,\ \omega_y,\ \omega_z\}$, $\mathbf{x} \to \mathbf{x}\,a_s$ with $a_s = \sqrt{\frac{\hbar}{m\omega_m}}$, $\psi_l \to \sqrt{N}\psi_l/a_s^{3/2}$ $(l=-1,0,1)$, we get the dimensionless coupled GPEs from (1.1)-(1.3) as [30, 32, 9]:

$$i\partial_t\psi_1(\mathbf{x},t) = \left[-\frac{1}{2}\nabla^2 + V(\mathbf{x}) + (\beta_n+\beta_s)\left(|\psi_1|^2+|\psi_0|^2\right) + (\beta_n-\beta_s)|\psi_{-1}|^2\right]\psi_1$$
$$+\beta_s\,\bar{\psi}_{-1}\,\psi_0^2, \tag{1.6}$$
$$i\partial_t\psi_0(\mathbf{x},t) = \left[-\frac{1}{2}\nabla^2 + V(\mathbf{x}) + (\beta_n+\beta_s)\left(|\psi_1|^2+|\psi_{-1}|^2\right) + \beta_n|\psi_0|^2\right]\psi_0$$
$$+2\beta_s\,\psi_{-1}\,\bar{\psi}_0\,\psi_1, \tag{1.7}$$
$$i\partial_t\psi_{-1}(\mathbf{x},t) = \left[-\frac{1}{2}\nabla^2 + V(\mathbf{x}) + (\beta_n+\beta_s)\left(|\psi_{-1}|^2+|\psi_0|^2\right) + (\beta_n-\beta_s)|\psi_1|^2\right]\psi_{-1}$$
$$+\beta_s\,\psi_0^2\,\bar{\psi}_1; \tag{1.8}$$

where $\beta_n = \frac{N\,c_0}{a_s^3\hbar\omega_m} = \frac{4\pi N(a_0+2a_2)}{3a_s}$, $\beta_s = \frac{N\,c_2}{a_s^3\hbar\omega_m} = \frac{4\pi N(a_2-a_0)}{3a_s}$ and $V(\mathbf{x}) = \frac{1}{2}(\gamma_x^2x^2 + \gamma_y^2y^2 + \gamma_z^2z^2)$ with $\gamma_x = \frac{\omega_x}{\omega_m}$, $\gamma_y = \frac{\omega_y}{\omega_m}$ and $\gamma_z = \frac{\omega_z}{\omega_m}$. Similar as those in single

component BEC [24, 8, 3, 6], in a disk-shaped condensation, i.e. $\omega_x \approx \omega_y$ and $\omega_z \gg \omega_x$ ($\Longleftrightarrow \gamma_x = 1$, $\gamma_y \approx 1$ and $\gamma_z \gg 1$ with $\omega_m = \omega_x$), the 3D coupled GPEs (1.6)-(1.8) can be reduced to a 2D coupled GPEs; and in a cigar-shaped condensation, i.e. $\omega_y \gg \omega_x$ and $\omega_z \gg \omega_x$ ($\Longleftrightarrow \gamma_x = 1$, $\gamma_y \gg 1$ and $\gamma_z \gg 1$ with $\omega_m = \omega_x$), the 3D coupled GPEs (1.6)-(1.8) can be reduced to a 1D coupled GPEs. Thus here we consider the dimensionless coupled GPEs in d-dimensions ($d = 1, 2, 3$):

$$i\partial_t\psi_1(\mathbf{x},t) = \left[-\frac{1}{2}\nabla^2 + V(\mathbf{x}) + (\beta_n+\beta_s)\left(|\psi_1|^2+|\psi_0|^2\right) + (\beta_n-\beta_s)|\psi_{-1}|^2\right]\psi_1$$
$$+\beta_s\,\bar{\psi}_{-1}\,\psi_0^2, \tag{1.9}$$
$$i\partial_t\psi_0(\mathbf{x},t) = \left[-\frac{1}{2}\nabla^2 + V(\mathbf{x}) + (\beta_n+\beta_s)\left(|\psi_1|^2+|\psi_{-1}|^2\right) + \beta_n|\psi_0|^2\right]\psi_0$$
$$+2\beta_s\,\psi_{-1}\,\bar{\psi}_0\,\psi_1, \tag{1.10}$$
$$i\partial_t\psi_{-1}(\mathbf{x},t) = \left[-\frac{1}{2}\nabla^2 + V(\mathbf{x}) + (\beta_n+\beta_s)\left(|\psi_{-1}|^2+|\psi_0|^2\right) + (\beta_n-\beta_s)|\psi_1|^2\right]\psi_{-1}$$
$$+\beta_s\,\psi_0^2\,\bar{\psi}_1. \tag{1.11}$$

In the equations above, $V(\mathbf{x})$ is a real-valued potential whose shape is determined by the type of system under investigation, $\beta_n \propto N$ and $\beta_s \propto N$ correspond to the dimensionless mean-field (spin-independent) and spin-exchange interaction, respectively. Three important invariants of (1.9)-(1.11) are the *mass* (or normalization) of the wave function

$$N(\Psi(\cdot,t)) := \|\Psi(\cdot,t)\|^2 := \int_{\mathbb{R}^d}\sum_{l=-1}^{1}|\psi_l(\mathbf{x},t)|^2\,d\mathbf{x} \equiv N(\Psi(\cdot,0)) = 1, \qquad t \ge 0, \tag{1.12}$$

the *magnetization* (with $-1 \le M \le 1$)

$$M(\Psi(\cdot,t)) := \int_{\mathbb{R}^d}\left[|\psi_1(\mathbf{x},t)|^2 - |\psi_{-1}(\mathbf{x},t)|^2\right]d\mathbf{x} \equiv M(\Psi(\cdot,0)) = M \tag{1.13}$$

and the energy per particle

$$E(\Psi(\cdot,t)) = \int_{\mathbb{R}^d}\Bigg\{\sum_{l=-1}^{1}\left(\frac{1}{2}|\nabla\psi_l|^2 + V(\mathbf{x})|\psi_l|^2\right) + (\beta_n-\beta_s)|\psi_1|^2|\psi_{-1}|^2$$
$$+\frac{\beta_n}{2}|\psi_0|^4 + \frac{\beta_n+\beta_s}{2}\left[|\psi_1|^4+|\psi_{-1}|^4+2|\psi_0|^2\left(|\psi_1|^2+|\psi_{-1}|^2\right)\right]$$
$$+\beta_s\left(\bar{\psi}_{-1}\psi_0^2\bar{\psi}_1 + \psi_{-1}\bar{\psi}_0^2\psi_1\right)\Bigg\}\,d\mathbf{x} \equiv E(\Psi(\cdot,0)), \qquad t \ge 0. \tag{1.14}$$

A fundamental problem in studying BEC is to find the condensate stationary states $\Phi(\mathbf{x})$, in particular the ground state which is the lowest energy stationary state. In other words, the ground state, $\Phi_g(\mathbf{x})$, is obtained from the minimization of the energy functional subject to the conservation of total mass and magnetization:

Find ($\Phi_g \in S$) such that

$$E_g := E(\Phi_g) = \min_{\Phi\in S} E(\Phi), \tag{1.15}$$

where the nonconvex set S is defined as

$$S = \left\{ \Phi = (\phi_1, \phi_0, \phi_{-1})^T \mid \|\Phi\| = 1,\ \int_{\mathbb{R}^d} \left[|\phi_1(\mathbf{x})|^2 - |\phi_{-1}(\mathbf{x})|^2 \right] = M,\ E(\Phi) < \infty \right\}. \tag{1.16}$$

This is a nonconvex minimization problem. When $\beta_n \geq 0$ and $\beta_n \geq |\beta_s|$ and $\lim_{|\mathbf{x}|\to\infty} V(\mathbf{x}) = \infty$, the existence of a minimizer of the nonconvex minimization problem (1.15) follows from the standard theory [25]. For understanding the uniqueness question note that $E(\alpha \cdot \Phi_g) = E(\Phi_g)$ for all $\alpha = \left(e^{i\theta_1}, e^{i\theta_0}, e^{i\theta_{-1}}\right)^T$ with $\theta_1 + \theta_{-1} = 2\theta_0$. Thus additional constraints have to be introduced to show the uniqueness.

As derived in [9], by defining the Lagrangian

$$\mathcal{L}(\Phi, \mu, \lambda) := E(\Phi) - \mu \left(\|\phi_1\|^2 + \|\phi_0\|^2 + \|\phi_{-1}\|^2 - 1 \right) - \lambda \left(\|\phi_1\|^2 - \|\phi_{-1}\|^2 - M \right), \tag{1.17}$$

we get the Euler-Lagrange equations associated to the minimization problem (1.15):

$$\begin{aligned} (\mu + \lambda)\, \phi_1(\mathbf{x}) = &\left[-\frac{1}{2}\nabla^2 + V(\mathbf{x}) + (\beta_n + \beta_s) \left(|\phi_1|^2 + |\phi_0|^2 \right) + (\beta_n - \beta_s) |\phi_{-1}|^2 \right] \phi_1 \\ &+ \beta_s\, \bar{\phi}_{-1}\, \phi_0^2 := H_1\, \phi_1, \end{aligned} \tag{1.18}$$

$$\begin{aligned} \mu\, \phi_0(\mathbf{x}) = &\left[-\frac{1}{2}\nabla^2 + V(\mathbf{x}) + (\beta_n + \beta_s) \left(|\phi_1|^2 + |\phi_{-1}|^2 \right) + \beta_n |\phi_0|^2 \right] \phi_0 \\ &+ 2\beta_s\, \phi_{-1}\, \bar{\phi}_0\, \phi_1 := H_0\, \phi_0, \end{aligned} \tag{1.19}$$

$$\begin{aligned} (\mu - \lambda)\, \phi_{-1}(\mathbf{x}) = &\left[-\frac{1}{2}\nabla^2 + V(\mathbf{x}) + (\beta_n + \beta_s) \left(|\phi_{-1}|^2 + |\phi_0|^2 \right) + (\beta_n - \beta_s) |\phi_1|^2 \right] \phi_{-1} \\ &+ \beta_s\, \phi_0^2\, \bar{\phi}_1 := H_{-1}\, \phi_{-1}. \end{aligned} \tag{1.20}$$

Here μ and λ are the Lagrange multipliers (or chemical potentials) of the coupled GPEs (1.9)-(1.11). In addition, (1.18)-(1.20) is also a nonlinear eigenvalue problem with two constraints

$$\|\Phi\|^2 := \int_{\mathbb{R}^d} |\Phi(\mathbf{x})|^2\, d\mathbf{x} = \int_{\mathbb{R}^d} \sum_{l=-1}^{1} |\phi_l(\mathbf{x})|^2\, d\mathbf{x} := \sum_{l=-1}^{1} \|\phi_l\|^2 = 1, \tag{1.21}$$

$$\|\phi_1\|^2 - \|\phi_{-1}\|^2 := \int_{\mathbb{R}^d} \left[|\phi_1(\mathbf{x})|^2 - |\phi_{-1}(\mathbf{x})|^2 \right] d\mathbf{x} = M. \tag{1.22}$$

In fact, the nonlinear eigenvalue problem (1.18)-(1.20) can also be obtained from the coupled GPEs (1.9)-(1.11) by plugging $\psi_l(\mathbf{x}, t) = e^{-i\mu_l t} \phi_l(\mathbf{x})$ $(l = 1, 0, -1)$ with

$$\mu_1 = \mu + \lambda, \quad \mu_0 = \mu, \quad \mu_{-1} = \mu - \lambda \qquad \Longleftrightarrow \qquad \mu_1 + \mu_{-1} = 2\mu_0. \tag{1.23}$$

Thus it is also called as time-independent coupled GPEs. In physics literatures, any eigenfucntion Φ of the nonlinear eigenvalue problem (1.18)-(1.20) under constraints (1.21) and (1.22), whose energy is larger than the energy of the ground state is called as an excited state of the coupled GPEs (1.9)-(1.11).

A widely used numerical method for computing the ground state of a single component condensate is the imaginary time method followed by an appropriate

discretization scheme [15, 5, 3] to evolve the resulted gradient flow equation under normalization of the wavefunction, which is mathematically justified by using the normalized gradient flow [5, 3]. However, it is not obvious that this most popular and powerful normalized gradient flow (or imaginary time method) could be directly extended to compute the ground state of spin-1 BEC. The reason is that we only have two normalization conditions (i.e. the two constraints: conservation of total mass and magnetization) which are insufficient to determine the three projection constants for the three components of the wavefunction used in the normalization step. In physics literatures, the imaginary time method is still applied to compute the ground state of spin-1 BEC through the introduction of a random variable to choose the three projection parameters in the projection step [30, 32]. Of course, this is not a determinate and efficient way to compute the ground state of spin-1 BEC due to the choice of the random variable. Recently, Bao and Wang [9] have proposed a continuous normalized gradient flow (CNGF) for computing the ground state of spin-1 BEC. The CNGF is discretized by Crank-Nicolson finite difference method with a proper and very special way to deal with the nonlinear terms and thus the discretization scheme can be proved to be mass and magnetization conservative and energy diminishing in the discretized level [9]. However, at each time step, a fully nonlinear system must be solved which is a little tedious from computational point of view since the CNGF is an integral-differential equations (see details in (A.1)-(A.9)) which involves implicitly the Lagrange multipliers in the normalized gradient flow evolution [9]. The aim of this paper is to introduce a third normalization condition based on the relation between the chemical potentials of spin-1 BEC, in addition to the two existing normalization conditions given by the conservation of the total mass and magnetization. Thus we can completely determine the three projection constants used in the normalization step for the normalized gradient flow. This allows us to develop the most popular and powerful normalized gradient flow or imaginary time method to compute the ground state of spin-1 BEC.

The paper is organized as follows. In section 2, the normalized gradient flow is constructed by introducing the third projection or normalization condition for computing the ground state of spin-1 BEC. In section 3, the backward-forward Euler sine-pseudospectral method (BESP) is presented to discretize the normalized gradient flow. In section 4, ground states of spin-1 BEC are reported with ferromagnetic/antiferromagnetic interaction and harmonic/optical lattice potential in one/three dimensions, respectively. Finally, some conclusions are drawn in section 5.

2. The normalized gradient flow. In this section, we will construct the normalized gradient flow for computing the ground state of spin-1 BEC by introducing the third normalization condition.

Various algorithms for computing the minimizer of the nonconvex minimization problem (1.15) have been studied in literature. For instance, a continuous normalized gradient flow (CNGF) and its discretization that preserve the total mass and magnetization conservation and energy diminishing properties were presented in [9]. Perhaps one of the more popular and efficient techniques for dealing with the normalization constraints in (1.16) is through the following construction: choose a time step $k = \Delta t > 0$ and denote time steps as $t_n = n\ k$ for $n = 0, 1, 2, \cdots$. To adapt an efficient algorithm for the solution of the usual gradient flow to the minimization problem under constraints, it is natural to consider the following splitting (or projection) scheme, which was widely used in the physics literature for computing the

ground state of BECs:

$$\partial_t \phi_1(\mathbf{x},t) = \left[\frac{1}{2}\nabla^2 - V(\mathbf{x}) - (\beta_n+\beta_s)\left(|\phi_1|^2+|\phi_0|^2\right) - (\beta_n-\beta_s)|\phi_{-1}|^2\right]\phi_1$$

$$-\beta_s\,\bar{\phi}_{-1}\,\phi_0^2, \tag{2.1}$$

$$\partial_t \phi_0(\mathbf{x},t) = \left[\frac{1}{2}\nabla^2 - V(\mathbf{x}) - (\beta_n+\beta_s)\left(|\phi_1|^2+|\phi_{-1}|^2\right) - \beta_n|\phi_0|^2\right]\phi_0$$

$$-2\beta_s\,\phi_{-1}\,\bar{\phi}_0\,\phi_1, \qquad \mathbf{x}\in\mathbb{R}^d, \quad t_{n-1}\le t<t_n, \qquad n\ge 1, \tag{2.2}$$

$$\partial_t \phi_{-1}(\mathbf{x},t) = \left[\frac{1}{2}\nabla^2 - V(\mathbf{x}) - (\beta_n+\beta_s)\left(|\phi_{-1}|^2+|\phi_0|^2\right) - (\beta_n-\beta_s)|\phi_1|^2\right]\phi_{-1}$$

$$-\beta_s\,\phi_0^2\,\bar{\phi}_1; \tag{2.3}$$

followed by a projection step as

$$\phi_1(\mathbf{x},t_n) := \phi_1(\mathbf{x},t_n^+) = \sigma_1^n\;\phi_1(\mathbf{x},t_n^-), \tag{2.4}$$

$$\phi_0(\mathbf{x},t_n) := \phi_0(\mathbf{x},t_n^+) = \sigma_0^n\;\phi_0(\mathbf{x},t_n^-), \qquad \mathbf{x}\in\mathbb{R}^d, \qquad n\ge 1, \tag{2.5}$$

$$\phi_{-1}(\mathbf{x},t_n) := \phi_{-1}(\mathbf{x},t_n^+) = \sigma_{-1}^n\;\phi_{-1}(\mathbf{x},t_n^-); \tag{2.6}$$

where $\phi_l(\mathbf{x},t_n^\pm) = \lim_{t\to t_n^\pm}\phi_l(\mathbf{x},t)$ $(l=-1,0,1)$ and σ_l^n $(l=-1,0,1)$ are projection constants and they are chosen such that

$$\|\Phi(\cdot,t_n)\|^2 = \sum_{l=-1}^{1}\|\phi_l(\cdot,t_n)\|^2 = 1, \qquad \|\phi_1(\cdot,t_n)\|^2 - \|\phi_{-1}(\cdot,t_n)\|^2 = M. \tag{2.7}$$

In fact, the gradient flow (2.1)-(2.3) can be viewed as applying the steepest decent method to the energy functional $E(\Phi)$ in (1.14) without constraints, and (2.4)-(2.6) project the solution back to the unit sphere S in order to satisfy the constraints in (1.16). In addition, (2.1)-(2.3) can also be obtained from the coupled GPEs (1.9)-(1.11) by the change of variable $t\to -i\,t$, that is why the algorithm is usually called as the imaginary time method in the physics literatures [15, 5, 3].

Plugging (2.4)-(2.6) into (2.7), we obtain

$$\sum_{l=-1}^{1}\left(\sigma_l^n\right)^2\|\phi_l(\cdot,t_n^-)\|^2 = 1, \tag{2.8}$$

$$\left(\sigma_1^n\right)^2\|\phi_1(\cdot,t_n^-)\|^2 - \left(\sigma_{-1}^n\right)^2\|\phi_{-1}(\cdot,t_n^-)\|^2 = M. \tag{2.9}$$

There are three unknowns and only two equations in the above nonlinear system, so the solution is undetermined! In order to determine the projection constants σ_l^n $(l=-1,0,1)$, we need to find an additional equation. Based on the relation between the chemical potentials in (1.23) and the continuous normalized gradient flow proposed in [9] for computing the ground state of spin-1 BEC, see details in Appendix A, we propose to use the following equation as the third normalization condition

$$\sigma_1^n\;\sigma_{-1}^n = \left(\sigma_0^n\right)^2. \tag{2.10}$$

Solving the nonlinear system (2.8), (2.9) and (2.10), see details in Appendix B, we get explicitly the projection constants as

$$\sigma_0^n = \frac{\sqrt{1-M^2}}{\left[\|\phi_0(\cdot,t_n^-)\|^2 + \sqrt{4(1-M^2)\|\phi_1(\cdot,t_n^-)\|^2\|\phi_{-1}(\cdot,t_n^-)\|^2 + M^2\|\phi_0(\cdot,t_n^-)\|^4}\right]^{1/2}}, \tag{2.11}$$

(2.12)
$$\sigma_1^n = \frac{\sqrt{1+M-(\sigma_0^n)^2\|\phi_0(\cdot,t_n^-)\|^2}}{\sqrt{2}\ \|\phi_1(\cdot,t_n^-)\|}, \qquad \sigma_{-1}^n = \frac{\sqrt{1-M-(\sigma_0^n)^2\|\phi_0(\cdot,t_n^-)\|^2}}{\sqrt{2}\ \|\phi_{-1}(\cdot,t_n^-)\|}.$$

From the numerical point of view, the gradient flow (2.1)-(2.3) can be solved via traditional techniques, and the normalization of the gradient flow is simply achieved by a projection at the end of each time step.

3. Backward-forward Euler sine-pseudospectral method. In this section, we will present the backward-forward Euler sine-pseudospectral method (BESP) to discretize the normalized gradient flow (2.1)-(2.3), (2.4)-(2.6) and (2.11)-(2.12).

Due to the trapping potential $V(\mathbf{x})$ given by (1.4), the solution $\Phi(\mathbf{x},t)$ decays to zero exponentially fast when $|\mathbf{x}| \to \infty$. Thus in practical computation, we truncate the problem into a bounded computational domain $\Omega_{\mathbf{x}}$ (chosen as an interval (a,b) in 1D, a rectangle $(a,b)\times(c,d)$ in 2D, and a box $(a,b)\times(c,d)\times(e,f)$ in 3D, with $|a|$, $|c|$, $|e|$, b, d and f sufficiently large) with homogeneous Dirichlet boundary conditions.

For simplicity of notation we introduce the method for the case of one spatial dimension ($d=1$) defined over the interval (a,b) with homogeneous Dirichlet boundary conditions. Generalization to higher dimension are straightforward for tensor product grids, and the results remain valid without modifications. For $d=1$, we choose the spatial mesh size $h=\Delta x>0$ with $h=(b-a)/M$ for M an even positive integer, and let the grid points be

$$x_l := a + j\ h, \qquad j = 0,1,\cdots,M.$$

Let $\Phi_j^n = (\phi_{1,j}^n, \phi_{0,j}^n, \phi_{-1,j}^n)^T$ be the approximation of $\Phi(x_j,t_n) = (\phi_1(x_j,t_n), \phi_0(x_j,t_n), \phi_{-1}(x_j,t_n))^T$ and Φ^n be the solution vector with component Φ_j^n. In the discretization, we use sine-pseudospectral method for spatial derivatives and backward/forward Euler scheme for linear/nonlinear terms in time discretization. The gradient flow (2.1)-(2.3) is discretized, for $j=1,2,\ldots,M-1$ and $n\ge 1$, as

$$\frac{\phi_{1,j}^* - \phi_{1,j}^{n-1}}{\Delta t} = \frac{1}{2}D_{xx}^s\phi_1^*|_{x=x_j} - \alpha_1\phi_{1,j}^* + G_{1,j}^{n-1}, \tag{3.1}$$

$$\frac{\phi_{0,j}^* - \phi_{0,j}^{n-1}}{\Delta t} = \frac{1}{2}D_{xx}^s\phi_0^*|_{x=x_j} - \alpha_0\phi_{0,j}^* + G_{0,j}^{n-1}, \qquad , \tag{3.2}$$

$$\frac{\phi_{-1,j}^* - \phi_{-1,j}^{n-1}}{\Delta t} = \frac{1}{2}D_{xx}^s\phi_{-1}^*|_{x=x_j} - \alpha_{-1}\phi_{-1,j}^* + G_{-1,j}^{n-1}; \tag{3.3}$$

where

$$\begin{aligned} G_{1,j}^{n-1} &= \left[\alpha_1 - V(x_j) - (\beta_n+\beta_s)\left(|\phi_{1,j}^{n-1}|^2 + |\phi_{0,j}^{n-1}|^2\right) - (\beta_n-\beta_s)|\phi_{-1,j}^{n-1}|^2\right]\phi_{1,j}^{n-1} \\ &\quad -\beta_s\,\bar{\phi}_{-1,j}^{n-1}\left(\phi_{0,j}^{n-1}\right)^2, \end{aligned} \tag{3.4}$$

$$\begin{aligned} G_{0,j}^{n-1} &= \left[\alpha_0 - V(x_j) - (\beta_n+\beta_s)\left(|\phi_{1,j}^{n-1}|^2 + |\phi_{-1,j}^{n-1}|^2\right) - \beta_n|\phi_{0,j}^{n-1}|^2\right]\phi_{0,j}^{n-1} \\ &\quad -2\beta_s\,\phi_{-1,j}^{n-1}\,\bar{\phi}_{0,j}^{n-1}\,\phi_{1,j}^{n-1}, \end{aligned} \tag{3.5}$$

$$\begin{aligned} G_{-1,j}^{n-1} &= \left[\alpha_{-1} - V(x_j) - (\beta_n+\beta_s)\left(|\phi_{-1,j}^{n-1}|^2 + |\phi_{0,j}^{n-1}|^2\right) - (\beta_n-\beta_s)|\phi_{1,j}^{n-1}|^2\right]\phi_{-1,j}^{n-1} \\ &\quad -\beta_s\left(\phi_{0,j}^{n-1}\right)^2\bar{\phi}_{1,j}^{n-1}. \end{aligned} \tag{3.6}$$

Here, D_{xx}^s, a pseudospectral differential operator approximation of ∂_{xx}, is defined as

$$D_{xx}^s U|_{x=x_j} = -\sum_{m=1}^{M-1} \mu_m^2 (\hat{U})_m \ \sin(\mu_m(x_j-a)), \qquad j=1,2,\cdots,M-1,$$

where $(\hat{U})_m$ $(m=1,2,\cdots,M-1)$, the sine transform coefficients of the vector $U=(U_0,U_1,\cdots,U_M)^T$ satisfying $U_0=U_M=0$, are defined as

$$\mu_m=\frac{\pi m}{b-a}, \qquad (\hat{U})_m=\frac{2}{M}\sum_{j=1}^{M-1} U_j \ \sin(\mu_m(x_j-a)), \quad m=1,2,\cdots,M-1;$$

and α_l $(l=-1,0,1)$ are the stabilization parameters which are chosen in the 'optimal' form (such that the time step can be chosen as large as possible) as [4]

$$\alpha_1=\frac{1}{2}\left(b_1^{\max}+b_1^{\min}\right), \quad \alpha_0=\frac{1}{2}\left(b_0^{\max}+b_0^{\min}\right), \quad \alpha_{-1}=\frac{1}{2}\left(b_{-1}^{\max}+b_{-1}^{\min}\right); \tag{3.7}$$

with

$$\begin{aligned}
b_1^{\max} &= \max_{1\le j\le M-1}\left[V(x_j)+(\beta_n+\beta_s)\left(|\phi_{1,j}^{n-1}|^2+|\phi_{0,j}^{n-1}|^2\right)+(\beta_n-\beta_s)|\phi_{-1,j}^{n-1}|^2\right],\\
b_1^{\min} &= \min_{1\le j\le M-1}\left[V(x_j)+(\beta_n+\beta_s)\left(|\phi_{1,j}^{n-1}|^2+|\phi_{0,j}^{n-1}|^2\right)+(\beta_n-\beta_s)|\phi_{-1,j}^{n-1}|^2\right],\\
b_0^{\max} &= \max_{1\le j\le M-1}\left[V(x_j)+(\beta_n+\beta_s)\left(|\phi_{1,j}^{n-1}|^2+|\phi_{-1,j}^{n-1}|^2\right)+\beta_n|\phi_{0,j}^{n-1}|^2\right],\\
b_0^{\min} &= \min_{1\le j\le M-1}\left[V(x_j)+(\beta_n+\beta_s)\left(|\phi_{1,j}^{n-1}|^2+|\phi_{-1,j}^{n-1}|^2\right)+\beta_n|\phi_{0,j}^{n-1}|^2\right],\\
b_{-1}^{\max} &= \max_{1\le j\le M-1}\left[V(x_j)+(\beta_n+\beta_s)\left(|\phi_{-1,j}^{n-1}|^2+|\phi_{0,j}^{n-1}|^2\right)+(\beta_n-\beta_s)|\phi_{1,j}^{n-1}|^2\right],\\
b_{-1}^{\min} &= \min_{1\le j\le M-1}\left[V(x_j)+(\beta_n+\beta_s)\left(|\phi_{-1,j}^{n-1}|^2+|\phi_{0,j}^{n-1}|^2\right)+(\beta_n-\beta_s)|\phi_{1,j}^{n-1}|^2\right].
\end{aligned}$$

The homogeneous Dirichlet boundary conditions are discretized as

$$\phi_{1,0}^*=\phi_{1,M}^*=\phi_{0,0}^*=\phi_{0,M}^*=\phi_{-1,0}^*=\phi_{-1,M}^*=0. \tag{3.8}$$

The projection step (2.4)-(2.4) is discretized, for $0\le j\le M$ and $n\ge 1$, as

$$\phi_{1,j}^n=\sigma_1^n\ \phi_{1,j}^*, \quad \phi_{0,j}^n=\sigma_0^n\ \phi_{0,j}^*, \quad \phi_{-1,j}^n=\sigma_{-1}^n\ \phi_{-1,j}^*, \tag{3.9}$$

where

$$\sigma_0^n=\frac{\sqrt{1-M^2}}{\left[\|\phi_0^*\|^2+\sqrt{4(1-M^2)\|\phi_1^*\|^2\|\phi_{-1}^*\|^2+M^2\|\phi_0^*\|^4}\right]^{1/2}}, \tag{3.10}$$

$$\sigma_1^n=\frac{\sqrt{1+M-\alpha_0^2\|\phi_0^*\|^2}}{\sqrt{2}\ \|\phi_1^*\|}, \qquad \sigma_{-1}^n=\frac{\sqrt{1-M-\alpha_0^2\|\phi_0^*\|^2}}{\sqrt{2}\ \|\phi_{-1}^*\|}; \tag{3.11}$$

with

$$\|\phi_1^*\|^2=h\sum_{j=1}^{M-1}|\phi_{1,j}^*|^2, \qquad \|\phi_0^*\|^2=h\sum_{j=1}^{M-1}|\phi_{0,j}^*|^2, \qquad \|\phi_{-1}^*\|^2=h\sum_{j=1}^{M-1}|\phi_{-1,j}^*|^2.$$

The initial data (A.10) is discretized as

$$\phi_{l,j}^0 = \phi_l(x_j, 0), \qquad j = 0, 1, 2, \cdots, M, \qquad l = -1, 0, 1.$$

The linear system (3.1)-(3.3) can be solved very efficiently by using the fast sine transform. In fact, take discrete sine transform at both sides, we get

$$\frac{1}{\Delta t}\left[(\hat{\phi}_1^*)_m - (\hat{\phi}_1^{n-1})_m\right] = -\left[\frac{1}{2}\mu_m^2 + \alpha_1\right](\hat{\phi}_1^*)_m + (\hat{G}_1^{n-1})_m, \tag{3.12}$$

$$\frac{1}{\Delta t}\left[(\hat{\phi}_0^*)_m - (\hat{\phi}_0^{n-1})_m\right] = -\left[\frac{1}{2}\mu_m^2 + \alpha_0\right](\hat{\phi}_0^*)_m + (\hat{G}_0^{n-1})_m, \quad 1 \le m < M, \tag{3.13}$$

$$\frac{1}{\Delta t}\left[(\hat{\phi}_{-1}^*)_m - (\hat{\phi}_{-1}^{n-1})_m\right] = -\left[\frac{1}{2}\mu_m^2 + \alpha_{-1}\right](\hat{\phi}_{-1}^*)_m + (\hat{G}_{-1}^{n-1})_m. \tag{3.14}$$

Solve the above system in the phase space, we obtain

$$(\hat{\phi}_1^*)_m = \frac{1}{1 + \Delta t\,[\alpha_1 + \mu_m^2/2]}\left[(\hat{\phi}_1^{n-1})_m + (\hat{G}_1^{n-1})_m\right], \tag{3.15}$$

$$(\hat{\phi}_0^*)_m = \frac{1}{1 + \Delta t\,[\alpha_1 + \mu_m^2/2]}\left[(\hat{\phi}_0^{n-1})_m + (\hat{G}_0^{n-1})_m\right], \quad 1 \le m < M, \tag{3.16}$$

$$(\hat{\phi}_{-1}^*)_m = \frac{1}{1 + \Delta t\,[\alpha_1 + \mu_m^2/2]}\left[(\hat{\phi}_{-1}^{n-1})_m + (\hat{G}_{-1}^{n-1})_m\right]. \tag{3.17}$$

REMARK 3.1. *The gradient flow (2.1)-(2.3) can also be discretized by using the backward Euler finite difference method proposed in [5] or the backward Euler sine-pseudospectral method proposed in [4] for computing the ground state of one-component BEC.*

4. Numerical Results. In this section, we first show that the ground states computed by our new numerical method are independent of the choice of the initial data in (A.10) and verify numerically the energy diminishing property of the method. Finally, we apply the method to compute the ground state of spin-1 BEC with different interactions and trapping potentials. In our computations, the ground state is reached by using the numerical method (3.1)-(3.3), (3.9)-(3.11) when $\|\Phi_h^{n+1} - \Phi_h^n\| \le \varepsilon := 10^{-7}$. In addition, in the ground state of spin-1 BEC, we have $M \leftrightarrow -M \iff \phi_1 \leftrightarrow \phi_{-1}$, thus we only present results for $0 \le M \le 1$.

4.1. Choice of initial data. In our tests, two typical physical experiments are considered:

- Case I. With ferromagnetic interaction, e.g. ^{87}Rb confined in a cigar-shaped trapping potential with parameters: $m = 1.443 \times 10^{-25}$[kg], $a_0 = 5.387$[nm], $a_2 = 5.313$[nm], $\omega_x = 2\pi \times 20$[Hz], $\omega_y = \omega_z = 2\pi \times 400$[Hz]. This suggests us to use dimensionless quantities in (1.9)-(1.11) for our computations as: $d = 1$, $V(x) = x^2/2$, $\beta_n \approx \frac{4\pi(a_0+2a_2)N}{3a_s}\frac{\sqrt{\omega_y\omega_z}}{2\pi\omega_x} = 0.0885N$ and $\beta_s \approx \frac{4\pi(a_2-a_0)N}{3a_s}\frac{\sqrt{\omega_y\omega_z}}{2\pi\omega_x} = -0.00041N$ with N the total number of atoms in the condensate and the dimensionless length unit $a_s = \sqrt{\hbar/m\omega_x} = 2.4116 \times 10^{-6}$ [m] and time unit $t_s = 1/\omega_x = 0.007958$[s].
- Case II. With antiferromagnetic interaction, e.g. ^{23}Na confined in a cigar-shaped trapping potential with parameters: $m = 3.816 \times 10^{-26}$[kg], $a_0 = 2.646$[nm], $a_2 = 2.911$[nm], $\omega_x = 2\pi \times 20$[Hz], $\omega_y = \omega_z = 2\pi \times 400$[Hz]. Again, this suggests us to use the following dimensionless quantities in our

computations: $d = 1$, $V(x) = x^2/2$, $\beta_n \approx 0.0241N$ and $\beta_s \approx 0.00075N$ with the dimensionless length unit $a_s = 4.6896 \times 10^{-6}$ [m] and time unit $t_s = 0.007958$[s].

We first test that the converged solution is independent of different choices of the initial data in (A.10) and energy diminishing property of the normalized gradient flow. In order to do so, we choose the initial data in (A.10) as

- Gaussian profiles satisfying the constraints in (1.16) initially, i.e.

$$\phi_1(x,0) = \frac{\sqrt{0.5(1+M-\kappa)}}{\pi^{1/4}} e^{-x^2/2}, \tag{4.1}$$

$$\phi_0(x,0) = \frac{\sqrt{\kappa}}{\pi^{1/4}} e^{-x^2/2}, \qquad -\infty < x < \infty, \tag{4.2}$$

$$\phi_{-1}(x,0) = \frac{\sqrt{0.5(1-M-\kappa)}}{\pi^{1/4}} e^{-x^2/2}, \tag{4.3}$$

  where κ is a constant satisfying $0 < \kappa < 1 - |M|$.
- Unnormalized Gaussian profiles, i.e.

$$\phi_1(x,0) = \phi_0(x,0) = \phi_{-1}(x,0) = e^{-x^2/2}, \qquad \infty < x < \infty. \tag{4.4}$$

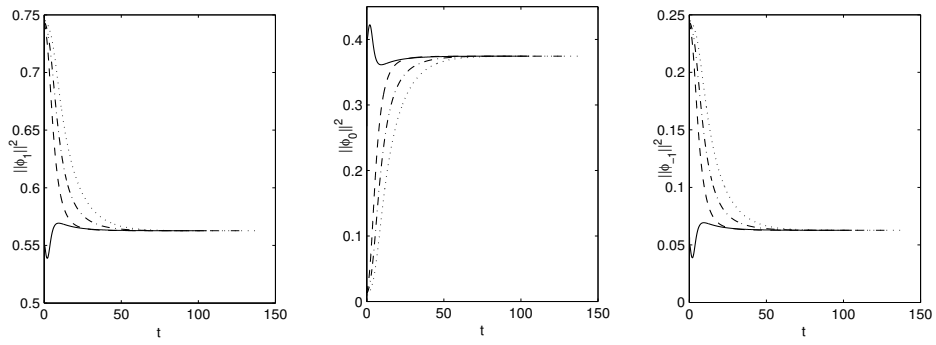

FIG. 4.1. *Time evolution of $N_1 = \|\phi_1(\cdot,t)\|^2$ ('left'), $N_0 = \|\phi_0(\cdot,t)\|^2$ ('middle') and $N_{-1} = \|\phi_{-1}(\cdot,t)\|^2$ ('right') by our method (2.4)-(2.6) for ^{87}Rb in Case I with $M = 0.5$ and $N = 10^4$ to analyze the convergence of different initial data in (4.4) (solid line) and (4.1)-(4.3) with $\kappa = 0.1$ (dotted line), $\kappa = 0.2$ (dash-dot line) and $\kappa = 0.4$ (dashed line), respectively.*

We solve the problem (1.15) by our method on $[-16, 16]$ with time step $\Delta t = 0.005$ and mesh size $h = 1/64$ for different values of κ in (4.1)-(4.3). Figure 4.1 plots time evolution of $N_l(t) := \|\phi_l(\cdot,t)\|^2$ $(l = 1, 0, -1)$ for ^{87}Rb in Case I with $M = 0.5$ and $N = 10^4$ for different choices of the initial data in (4.4) and (4.1)-(4.3), and Figure 4.2 shows similar results for ^{23}Na in Case II. In addition, Figure 4.3 depicts time evolution of the energy for the two cases with $M = 0.5$ and $N = 10^4$ for different choices of the initial data in (4.4).

From Figs. 4.1 and 4.2, we can see that the converged ground states are independent of the choice of initial data. In fact, based on our extensive numerical experiments on other types of initial data (not shown here for brevity), our numerical method always gives the ground state if all the three components in the initial data are chosen as nonnegative functions. In addition, Fig. 4.3 demonstrates the energy diminishing property of the normalized gradient flow and its full discretization when

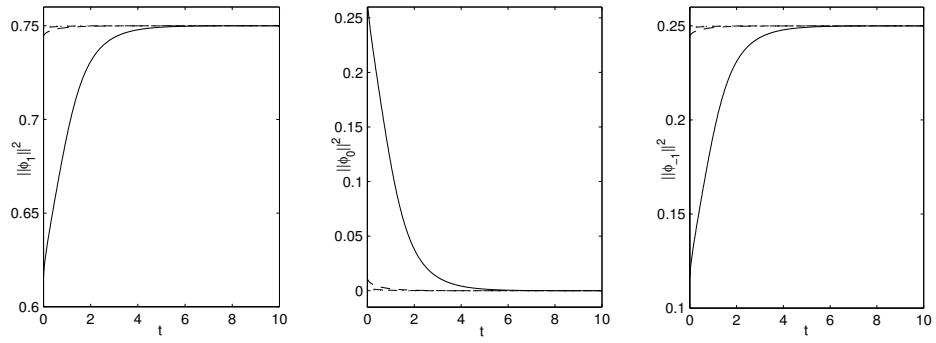

FIG. 4.2. *Time evolution of* $N_1 = \|\phi_1(\cdot,t)\|^2$ *('left'),* $N_0 = \|\phi_0(\cdot,t)\|^2$ *('middle') and* $N_{-1} = \|\phi_{-1}(\cdot,t)\|^2$ *('right') by our method (2.4)-(2.6) for* ^{23}Na *in Case II with* $M = 0.5$*, and* $N = 10^4$ *to analyze the convergence of different initial data in (4.4) (solid line) and (4.1)-(4.3) with* $\kappa = 0.1$ *(dotted line),* $\kappa = 0.2$ *(dash-dot line) and* $\kappa = 0.4$ *(dashed line), respectively.*

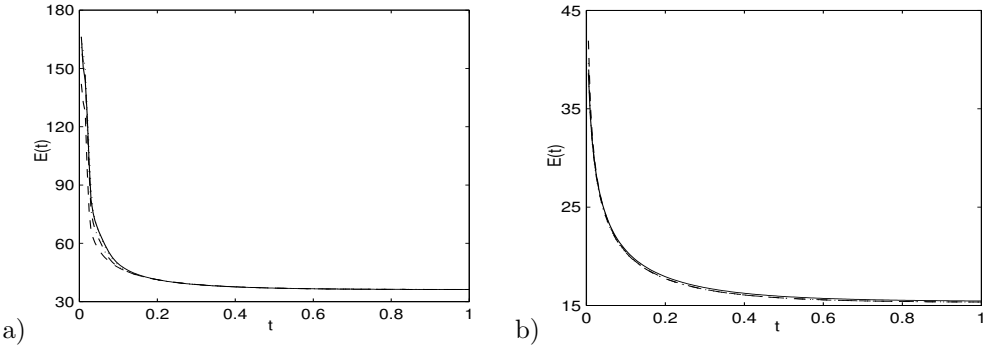

FIG. 4.3. *Time evolution of the energy by our method (2.4)-(2.6) with* $M = 0.5$*, and* $N = 10^4$ *for a)* ^{87}Rb *in case I; and b)* ^{23}Na *in case II with different initial data in (4.4) (solid line) and (4.1)-(4.3) with* $\kappa = 0.1$ *(dotted line),* $\kappa = 0.2$ *(dash-dot line) and* $\kappa = 0.4$ *(dashed line), respectively.*

time step Δt is small. Based on our numerical experiments, for $0 \le M \le 1$, we suggest the initial data in (A.10) be chosen as: i) with ferromagnetic interaction, i.e. $\beta_s \le 0$

$$\phi_1(\mathbf{x}) = \frac{1}{2}\sqrt{1+3M}\,\phi_g^{\rm ap}(\mathbf{x}), \quad \phi_0(\mathbf{x}) = \sqrt{\frac{1-M}{2}}\,\phi_g^{\rm ap}(\mathbf{x}), \quad \phi_1(\mathbf{x}) = \frac{1}{2}\sqrt{1-M}\,\phi_g^{\rm ap}(\mathbf{x});$$

and ii) with antiferromagnetic interaction, i.e. $\beta_s > 0$

$$\phi_1(\mathbf{x}) = \sqrt{\frac{1+M}{2}}\,\phi_g^{\rm ap}(\mathbf{x}), \quad \phi_0(\mathbf{x}) = 0, \quad \phi_1(\mathbf{x}) = \sqrt{\frac{1-M}{2}}\,\phi_g^{\rm ap}(\mathbf{x});$$

where $\phi_g^{\rm ap}(\mathbf{x})$ can be chosen as the approximate ground state solution of single component BEC, e.g. the harmonic oscillator approximation when β_n small and the Thomas-Fermi approximation when $\beta_n \gg 1$ [5, 8, 7]. Based on these choices of initial data, we report the ground states computed by our numerical method.

Figure 4.4 shows the ground state solutions of ^{87}Rb in Case I with $N = 10^4$ for different magnetization M and Table 4.1 lists the corresponding ground state energies and their Lagrange multipliers (see their detailed formulation in Appendix

C). In addition, Figure 4.5 shows similar ground state solutions with $M = 0.5$ for different particle number N.

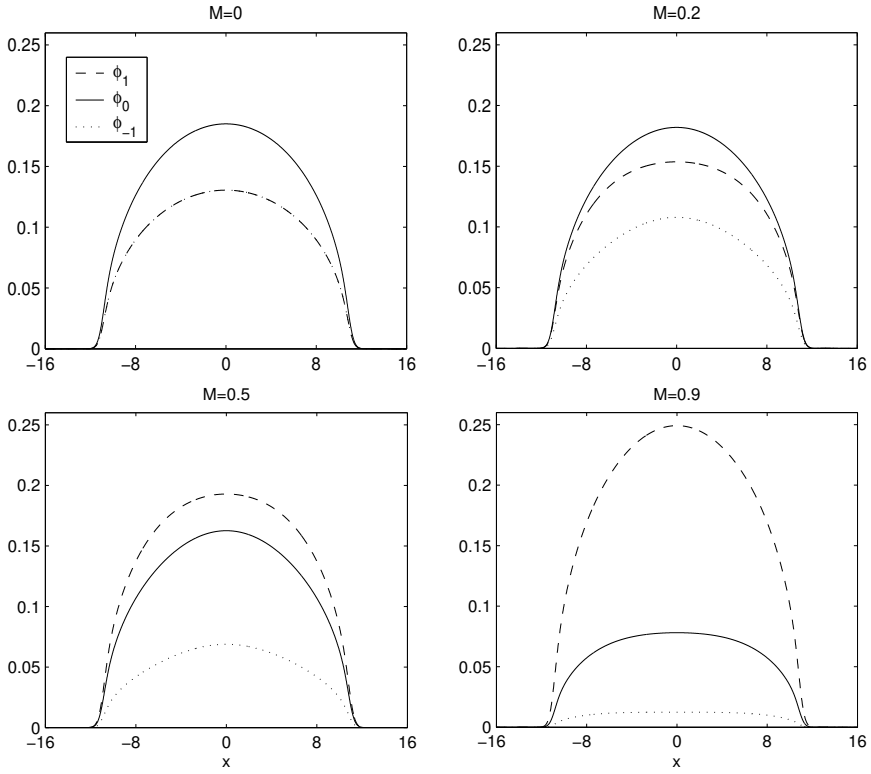

FIG. 4.4. *Wave functions of the ground state, i.e. $\phi_1(x)$ (dashed line), $\phi_0(x)$ (solid line) and $\phi_{-1}(x)$ (dotted line), of ^{87}Rb in Case I with fixed number of particles $N = 10^4$ for different magnetization $M = 0, 0.2, 0.5, 0.9$.*

Similarly, Figure 4.6 shows the ground state solutions of ^{23}Na in Case II with $N = 10^4$ for different magnetization M and Table 4.2 lists the corresponding ground state energies and their Lagrange multipliers. In addition, Figure 4.7 shows similar ground state solutions with $M = 0.5$ for different particle number N.

Figure 4.8 plots the mass of the three components in the spin-1 BEC ground states with $N = 10^4$ for different magnetization M, and Figure 4.9 depicts the energy and chemical potentials with $M = 0.5$ for different particle number N.

From Figs. 4.4-4.6 as well as Tabs. 4.1-4.2, we can draw the following conclusions: (i) For ferromagnetic interaction in the spin-1 BEC, i.e. $\beta_s \leq 0$, the three components in the ground state solutions are all positive functions (c.f. Figs. 4.4 and 4.5) ; while for antiferromagnetic interaction, i.e. $\beta_s \geq 0$, ϕ_1 and ϕ_{-1} are positive functions and $\phi_0 \equiv 0$ (c.f. Figs. 4.6 and 4.7). (ii) For ferromagnetic interaction in the spin-1 BEC, i.e. $\beta_s \leq 0$, for fixed number of particles N in the condensate, when the magnetization M increases from 0 to 1, the mass N_1 increases from 0.25 to 1, the mass N_{-1} decreases from 0.25 to 0 and the mass N_0 decreases from 0.5 to 0 (c.f. Fig. 4.9a); while for antiferromagnetic interaction, i.e. $\beta_s \geq 0$, N_1 increases from 0.5 to 1, N_{-1} decreases from 0.5 to 0 and $N_0 = 0$ (c.f. Fig. 4.9b). (iii) For ferromagnetic interaction in the spin-1 BEC, i.e. $\beta_s \leq 0$, for fixed number of particles N in the condensate,

M	E	μ	$\lambda(\times 10^{-5})$
0	36.1365	60.2139	0
0.1	36.1365	60.2139	1.574
0.2	36.1365	60.2139	1.621
0.3	36.1365	60.2139	1.702
0.4	36.1365	60.2139	1.827
0.5	36.1365	60.2139	2.014
0.6	36.1365	60.2139	2.218
0.7	36.1365	60.2139	2.062
0.8	36.1365	60.2139	2.081
0.9	36.1365	60.2139	2.521

TABLE 4.1

Ground state energy E and their chemical potentials μ and λ for ^{87}Rb in Case I with $N = 10^4$ for different magnetization M.

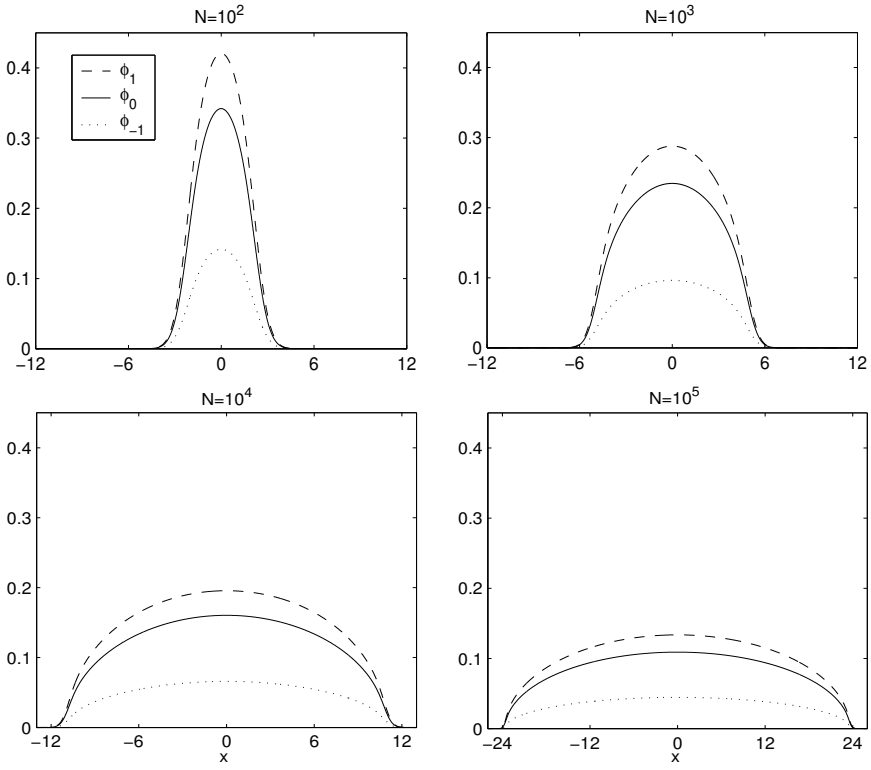

FIG. 4.5. *Wave functions of the ground state, i.e. $\phi_1(x)$ (dashed line), $\phi_0(x)$ (solid line) and $\phi_{-1}(x)$ (dotted line), of ^{87}Rb in Case I with magnetization $M = 0.5$ for different number of particles N.*

the energy and chemical potentials are almost independent of the magnetization (c.f. Tab. 4.1); while for antiferromagnetic interaction, i.e. $\beta_s \geq 0$, when the magnetization M increases from 0 to 1, the energy E increases and the main chemical potential μ decreases and the second chemical potential λ increases (c.f. Tab. 4.2). In both cases, for fixed magnetization M, when the number of particles N increases, the energy and

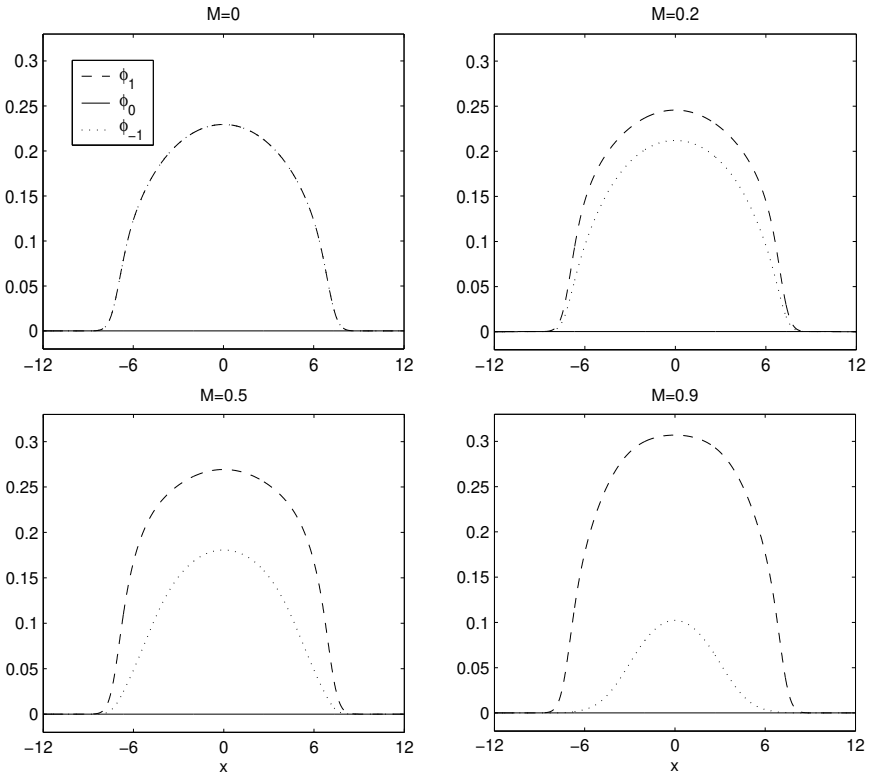

FIG. 4.6. *Wave functions of the ground state, i.e.* $\phi_1(x)$ *(dashed line),* $\phi_0(x)$ *(solid line) and* $\phi_{-1}(x)$ *(dotted line), of* ^{23}Na *in Case II with fixed number of particles* $N = 10^4$ *for different magnetization* $M = 0, 0.2, 0.5, 0.9$.

chemical potentials increase (c.f. Fig. 4.8). These observations agree with those obtained in [9] and [30] by different numerical methods.

4.2. Application in 1D with optical lattice potential. In this subsection, our method is applied to compute the ground state of spin-1 BEC in one dimension (1D) with an optical lattice potential. Again, two different interaction are considered:

- Case I. For ^{87}Rb with dimensionless quantities in (1.9)-(1.11) used as: $d = 1$, $V(x) = x^2/2 + 25\sin^2\left(\frac{\pi x}{4}\right)$, $\beta_n = 0.0885N$ and $\beta_s = -0.00041N$, with N the total number of atoms in the condensate and the dimensionless length unit $a_s = 2.4116 \times 10^{-6}$ [m] and time unit $t_s = 0.007958$[s].
- Case II. For ^{23}Na with dimensionless quantities in (1.9)-(1.11) used as: $d = 1$, $V(x) = x^2/2 + 25\sin^2\left(\frac{\pi x}{4}\right)$, $\beta_n = 0.0241N$ and $\beta_s = 0.00075N$, with N the total number of atoms in the condensate and the dimensionless length unit $a_s = 4.6896 \times 10^{-6}$ [m] and time unit $t_s = 0.007958$[s].

Figure 4.10 shows the ground state solutions of ^{87}Rb in Case I with $N = 10^4$ for different magnetization M and Table 4.3 lists the corresponding ground state energies and their Lagrange multipliers. Figure 4.11 and Table 4.4 show similar results for ^{23}Na in Case II.

From Figs. 4.10&4.11 and Tabs. 4.3&4.4, it can be seen that our method can be used in computing ground state of spin-1 BEC with general potential. In addition

M	E	μ	λ
0	15.2485	25.3857	0
0.1	15.2514	25.3847	0.0569
0.2	15.2599	25.3815	0.1142
0.3	15.2743	25.3762	0.1725
0.4	15.2945	25.3682	0.2325
0.5	15.3209	25.3572	0.2950
0.6	15.3537	25.3423	0.3611
0.7	15.3933	25.3220	0.4326
0.8	15.4405	25.2939	0.5121
0.9	15.4962	25.2527	0.6049

TABLE 4.2

Ground state energy E and their chemical potentials μ and λ for ^{23}Na in Case II with $N = 10^4$ for different magnetization M.

M	E	μ	$\lambda(\times 10^{-4})$
0	47.6944	73.0199	0
0.1	47.6944	73.0199	0.711
0.2	47.6944	73.0199	0.788
0.3	47.6944	73.0199	0.859
0.4	47.6944	73.0199	0.948
0.5	47.6944	73.0199	1.072
0.6	47.6944	73.0199	1.178
0.7	47.6944	73.0199	1.164
0.8	47.6944	73.0199	1.200
0.9	47.6944	73.0199	1.477

TABLE 4.3

Ground state energy E and their chemical potentials μ and λ for ^{87}Rb in Case I with $N = 10^4$ for different magnetization M in an optical lattice potential.

to that, similar conclusions as those in the end of previous subsection can also be observed in this case.

4.3. Applications in 3D with optical lattice potential. In this subsection, our method is applied to compute the ground state of spin-1 BEC in three dimensions (3D) with an optical lattice potential. Again, two different interaction are considered:

- Case I. For ^{87}Rb with dimensionless quantities in (1.9)-(1.11) used as: $d = 3$, $V(x) = \frac{1}{2}\left(x^2+y^2+z^2\right) + 100\left[\sin^2\left(\frac{\pi x}{2}\right) + \sin^2\left(\frac{\pi y}{2}\right) + \sin^2\left(\frac{\pi z}{2}\right)\right]$, $\beta_n = 0.0880N$ and $\beta_s = -0.00041N$, with N the total number of atoms in the condensate and the dimensionless length unit $a_s = \sqrt{\hbar/m\omega_x} = 7.6262 \times 10^{-7}$ [m] and time unit $t_s = 1/\omega_x = 7.9577 \times 10^{-4}$[s] (corresponding to physical trapping frequencies $\omega_x = \omega_y = \omega_z = 2\pi \times 200$[Hz]).
- Case II. For ^{23}Na with dimensionless quantities in (1.9)-(1.11) used as: $d = 3$, $V(x) = \frac{1}{2}\left(x^2+y^2+z^2\right) + 100\left[\sin^2\left(\frac{\pi x}{2}\right) + \sin^2\left(\frac{\pi y}{2}\right) + \sin^2\left(\frac{\pi z}{2}\right)\right]$, $\beta_n = 0.0239N$ and $\beta_s = 0.00075N$ with N the total number of atoms in the condensate and the dimensionless length unit $a_s = 1.4830 \times 10^{-6}$ [m] and time unit $t_s = 7.9577 \times 10^{-4}$[s](corresponding to physical trapping frequencies $\omega_x = \omega_y = \omega_z = 2\pi \times 200$[Hz]).

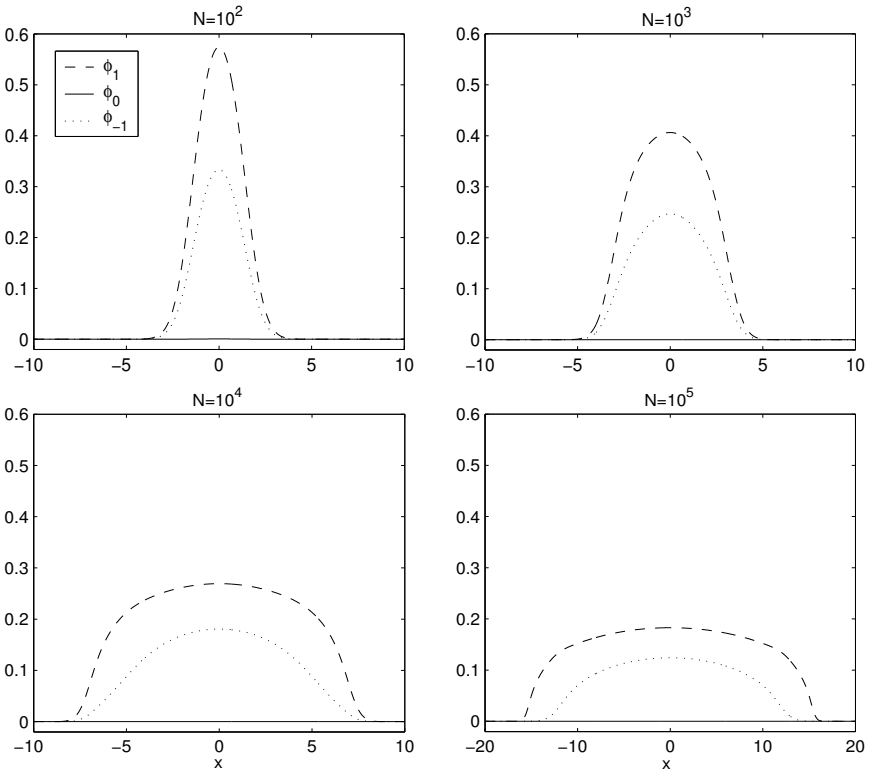

FIG. 4.7. *Wave functions of the ground state, i.e.* $\phi_1(x)$ *(dashed line),* $\phi_0(x)$ *(solid line) and* $\phi_{-1}(x)$ *(dotted line), of* ^{23}Na *in Case II with magnetization* $M = 0.5$ *for different number of particles* N.

Figure 4.12 shows the ground state solutions with $N = 10^4$ and $M = 0.5$ for the two cases.

From Fig. 4.12, we can see that our method can be used to compute the ground state of spin-1 BEC in 3D with general trapping potential.

5. Conclusions. We have proposed an efficient and accurate normalized gradient flow or imaginary time method to compute the ground state of spin-1 Bose-Einstein condensates by introducing a third normalization condition, in addition to the conservation of total particle number and the conservation of total magnetization. The condition is derived from the relationships between the chemical potentials of the three spinor components together with a splitting scheme applied to the continuous normalized gradient flows proposed to compute the ground state of spin-1 BEC. The backward-forward sine-pseudospectral method is applied to discretize the normalized gradient flow for practical computation. The ground state solutions and fraction of each component are reported for both ferromagnetic and antiferromagnetic interaction cases. The energy and chemical potentials of the condensate are also reported. In addition, the method may be further extended to other spinor condensate with higher degree of freedom as well as spinor condensate in the presence of external magnetic field, which will be our future study.

Finally, based on our extensive numerical experiments and results, we conjecture

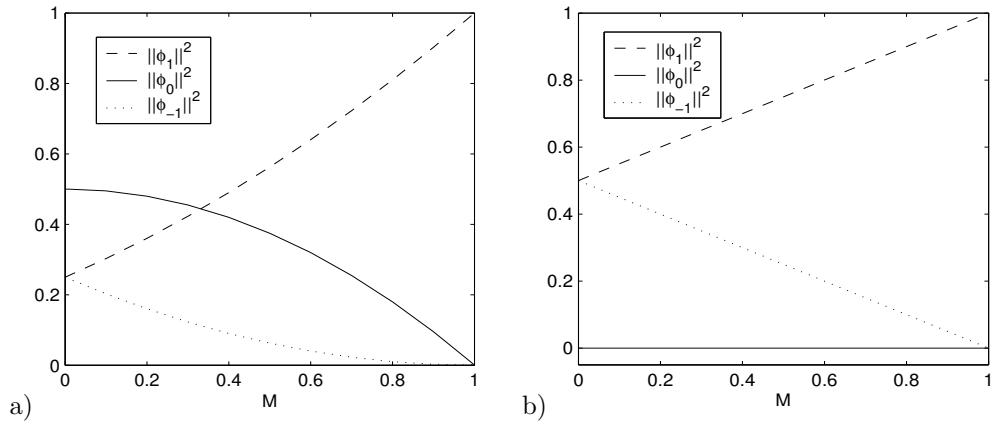

FIG. 4.8. *Mass of the three components of the ground state, i.e.* $N_l = \|\phi_l\|^2$ *(*$l = 1, 0, -1$*), of spin-1 BEC with fixed number of particles* $N = 10^4$ *for different magnetization* $0 \le M < 1$*. a) for* ^{87}*Rb in case I; and b) for* ^{23}*Na in case II.*

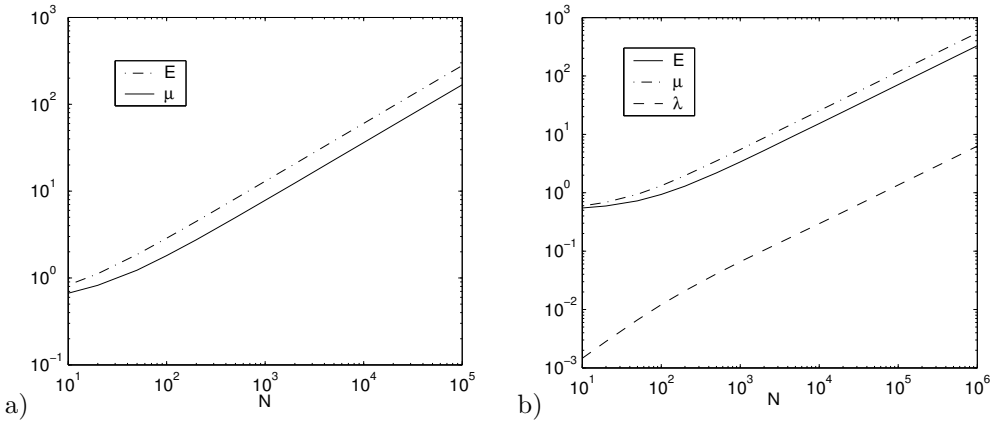

FIG. 4.9. *Energy E and chemical potentials* μ *and* λ *of spin-1 BEC with fixed magnetization* $M = 0.5$ *for different number of particles N. a) for* ^{87}*Rb in case I; and b) for* ^{23}*Na in case II.*

that when $\beta_n \ge 0$, $\beta_n \ge |\beta_s|$ and $V(\mathbf{x}) \ge 0$ satisfying $\lim_{|\mathbf{x}|\to\infty} V(\mathbf{x}) \to \infty$, there exists minimizer of the nonconvex minimization problem (1.15). In addition, when $\beta_s < 0$, positive minimizer (the three components are positive function) is unique; when $\beta_s > 0$, nonnegative minimizer (ϕ_1 and ϕ_{-1} are positive and $\phi_0 \equiv 0$) is unique. Rigorous mathematical justification are on-going.

Acknowledgment. We acknowledge support from the Ministry of Education of Singapore grant No. R-146-000-083-112.

Appendix A Derivation of the third projection equation (2.10)

In order to find the third projection or normalization equation used in the projection step of the normalized gradient flow, we first review the continuous normalized gradient flow (CNGF) constructed in [9] for computing the ground state of spin-1

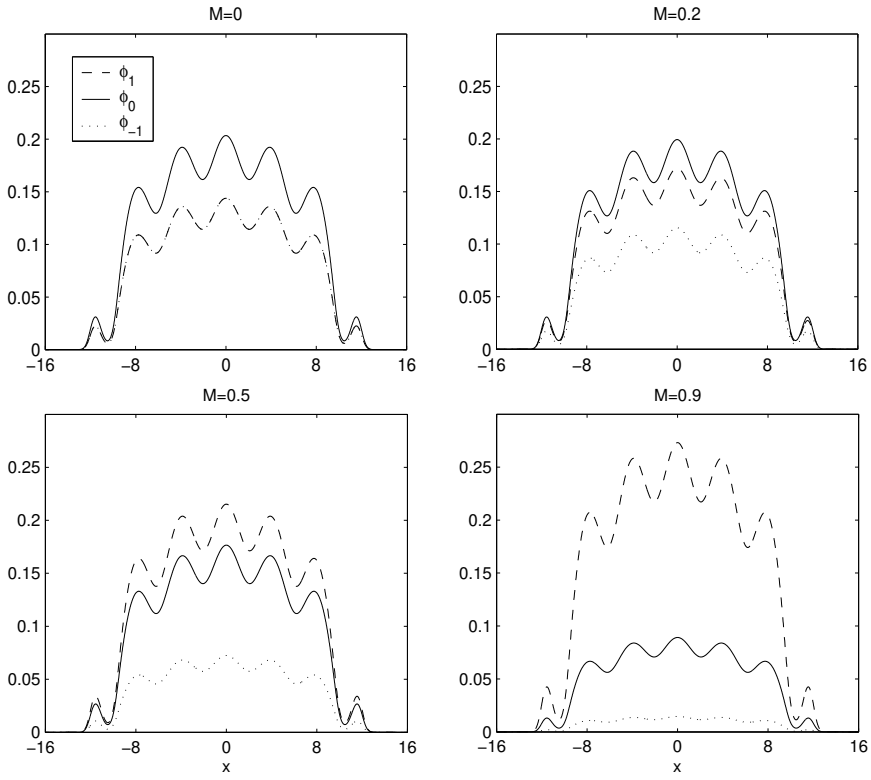

FIG. 4.10. *Wave functions of the ground state, i.e. $\phi_1(x)$ (dashed line), $\phi_0(x)$ (solid line) and $\phi_{-1}(x)$ (dotted line), of ^{87}Rb in Case I with fixed number of particles $N = 10^4$ for different magnetization $M = 0, 0.2, 0.5, 0.9$ in an optical lattice potential.*

BEC in (1.15):

$$\partial_t \phi_1(\mathbf{x},t) = \left[\frac{1}{2}\nabla^2 - V(\mathbf{x}) - (\beta_n+\beta_s)\left(|\phi_1|^2+|\phi_0|^2\right) - (\beta_n-\beta_s)|\phi_{-1}|^2\right]\phi_1$$
$$-\beta_s\,\bar{\phi}_{-1}\,\phi_0^2 + [\mu_\Phi(t)+\lambda_\Phi(t)]\,\phi_1, \tag{A.1}$$

$$\partial_t \phi_0(\mathbf{x},t) = \left[\frac{1}{2}\nabla^2 - V(\mathbf{x}) - (\beta_n+\beta_s)\left(|\phi_1|^2+|\phi_{-1}|^2\right) - \beta_n|\phi_0|^2\right]\phi_0$$
$$-2\beta_s\,\phi_{-1}\,\bar{\phi}_0\,\phi_1 + \mu_\Phi(t)\,\phi_0, \tag{A.2}$$

$$\partial_t \phi_{-1}(\mathbf{x},t) = \left[\frac{1}{2}\nabla^2 - V(\mathbf{x}) - (\beta_n+\beta_s)\left(|\phi_{-1}|^2+|\phi_0|^2\right) - (\beta_n-\beta_s)|\phi_1|^2\right]\phi_{-1}$$
$$-\beta_s\,\phi_0^2\,\bar{\phi}_1 + [\mu_\Phi(t)-\lambda_\Phi(t)]\,\phi_{-1}. \tag{A.3}$$

$\mu_\Phi(t)$ and $\lambda_\Phi(t)$ are chosen such that the above CNGF is mass (or normalization) and magnetization conservative and they are given as [9]

$$\mu_\Phi(t) = \frac{R_\Phi(t)D_\Phi(t) - M_\Phi(t)F_\Phi(t)}{N_\Phi(t)R_\Phi(t) - M_\Phi^2(t)}, \qquad \lambda_\Phi(t) = \frac{N_\Phi(t)F_\Phi(t) - M_\Phi(t)D_\Phi(t)}{N_\Phi(t)R_\Phi(t) - M_\Phi^2(t)}, \tag{A.4}$$

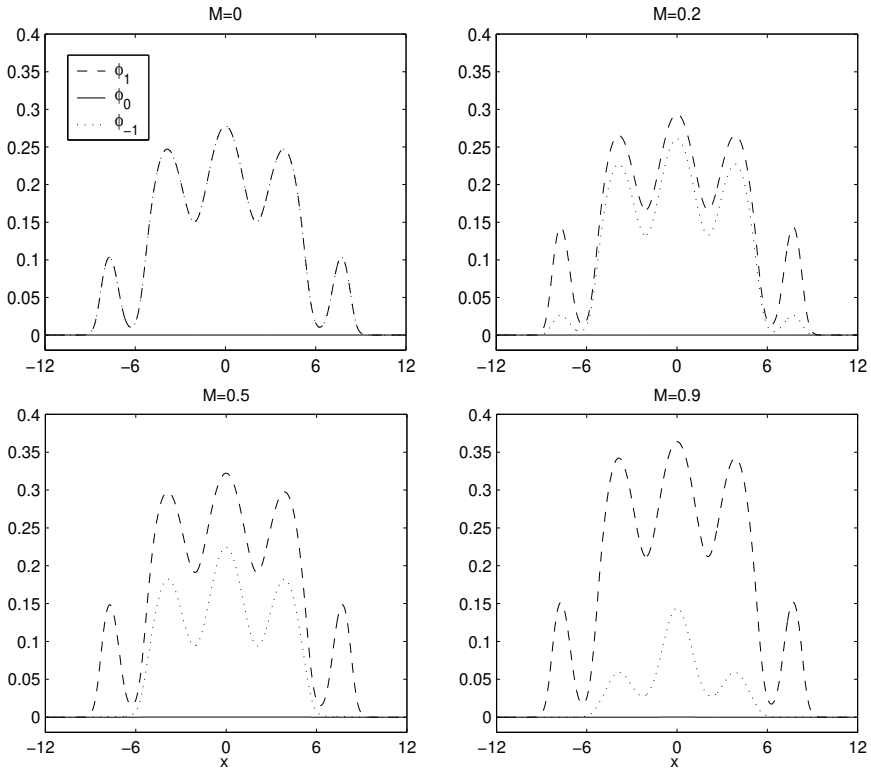

FIG. 4.11. *Wave functions of the ground state, i.e. $\phi_1(x)$ (dashed line), $\phi_0(x)$ (solid line) and $\phi_{-1}(x)$ (dotted line), of ^{23}Na in Case II with $N = 10^4$ for different magnetization $M = 0, 0.2, 0.5, 0.9$ in an optical lattice potential.*

FIG. 4.12. *Contour plots for the wave functions of the ground state, i.e. $\phi_1(x, y, 0)$ (top row), $\phi_0(x, y, 0)$ (middle row) and $\phi_{-1}(x, y, 0)$ (bottom row) with $N = 10^4$ and $M = 0.5$ in an optical lattice potential. Left column: for ^{87}Rb in Case I; and right column: for ^{23}Na in Case II.*

with

$$N_\Phi(t) = \int_{\mathbb{R}^d} \left[|\phi_{-1}(\mathbf{x},t)|^2 + |\phi_0(\mathbf{x},t)|^2 + |\phi_1(\mathbf{x},t)|^2\right] d\mathbf{x}, \tag{A.5}$$

$$M_\Phi(t) = \int_{\mathbb{R}^d} \left[|\phi_1(\mathbf{x},t)|^2 - |\phi_{-1}(\mathbf{x},t)|^2\right] \, d\mathbf{x}, \tag{A.6}$$

$$R_\Phi(t) = \int_{\mathbb{R}^d} \left[|\phi_1(\mathbf{x},t)|^2 + |\phi_{-1}(\mathbf{x},t)|^2\right] \, d\mathbf{x}, \tag{A.7}$$

$$\begin{aligned} D_\Phi(t) = \int_{\mathbb{R}^d} \Bigg\{ & \sum_{l=-1}^{1} \left(\frac{1}{2}|\nabla\phi_l|^2 + V(\mathbf{x})|\phi_l|^2\right) + 2(\beta_n - \beta_s)|\phi_1|^2|\phi_{-1}|^2 + \beta_n|\phi_0|^4 \\ & + (\beta_n + \beta_s)\Big[|\phi_1|^4 + |\phi_{-1}|^4 + 2|\phi_0|^2\left(|\phi_1|^2 + |\phi_{-1}|^2\right)\Big] \\ & + 2\beta_s\left(\bar{\phi}_{-1}\phi_0^2\bar{\phi}_1 + \phi_{-1}\bar{\phi}_0^2\phi_1\right)\Bigg\} \, d\mathbf{x}, \end{aligned} \tag{A.8}$$

M	E	μ	λ
0	25.6480	37.4489	0
0.1	25.6509	37.4476	0.0593
0.2	25.6597	37.4400	0.1197
0.3	25.6753	37.4248	0.1931
0.4	25.6983	37.4025	0.2687
0.5	25.7291	37.3775	0.3458
0.6	25.7676	37.3492	0.4252
0.7	25.8144	37.3167	0.5079
0.8	25.8696	37.2305	0.6920
0.9	25.9340	37.2305	0.6920

TABLE 4.4

Ground state energy E and their chemical potentials μ and λ for ^{23}Na in Case II with $N = 10^4$ for different magnetization M in an optical lattice potential.

$$F_\Phi(t) = \int_{\mathbb{R}^d} \Big\{ \frac{1}{2} \left(|\nabla\phi_1|^2 - |\nabla\phi_{-1}|^2 \right) + V(\mathbf{x}) \left(|\phi_1|^2 - |\phi_{-1}|^2 \right) + (\beta_n + \beta_s) \Big[|\phi_1|^4 - |\phi_{-1}|^4 + |\phi_0|^2 \left(|\phi_1|^2 - |\phi_{-1}|^2 \right) \Big] \Big\} \, d\mathbf{x}. \tag{A.9}$$

For the above CNGF, for any given initial data

$$\Phi(\mathbf{x}, 0) = (\phi_1(\mathbf{x}, 0), \phi_0(\mathbf{x}, 0), \phi_{-1}(\mathbf{x}, 0))^T := \Phi^{(0)}(\mathbf{x}), \qquad \mathbf{x} \in \mathbb{R}^d, \tag{A.10}$$

satisfying

$$N_\Phi(t = 0) := N_{\Phi^{(0)}} = 1, \qquad M_\Phi(t = 0) := M_{\Phi^{(0)}} = M, \tag{A.11}$$

it was proven that the total mass and magnetization are conservative and the energy is diminishing [9], i.e.

$$N_\Phi(t) \equiv 1, \quad M_\Phi(t) \equiv M, \quad E\left(\Phi(\cdot, t) \leq E\left(\Phi(\cdot, s)\right), \quad \text{for any } t \geq s \geq 0.\right.$$

The normalized gradient flow (2.1)-(2.6) can be viewed as applying a time-splitting scheme to the CNGF (A.1)-(A.3) and the projection step (2.4)-(2.6) is equivalent to solving the following nonlinear ordinary differential equations (ODEs):

$$\partial_t \phi_1(\mathbf{x}, t) = \left[\mu_\Phi(t) + \lambda_\Phi(t) \right] \phi_1, \tag{A.12}$$

$$\partial_t \phi_0(\mathbf{x}, t) = \mu_\Phi(t) \, \phi_0, \qquad t_{n-1} \leq t \leq t_n, \qquad n \geq 1, \tag{A.13}$$

$$\partial_t \phi_{-1}(\mathbf{x}, t) = \left[\mu_\Phi(t) - \lambda_\Phi(t) \right] \phi_{-1}. \tag{A.14}$$

The solution of the above ODEs can be expressed as

$$\phi_1(\mathbf{x}, t_n) = \exp\left(\int_{t_{n-1}}^{t_n} \left[\mu_\Phi(\tau) + \lambda_\Phi(\tau) \right] \, d\tau \right) \phi_1(\mathbf{x}, t_{n-1}), \tag{A.15}$$

$$\phi_0(\mathbf{x}, t_n) = \exp\left(\int_{t_{n-1}}^{t_n} \mu_\Phi(\tau) \, d\tau \right) \phi_0(\mathbf{x}, t_{n-1}), \tag{A.16}$$

$$\phi_{-1}(\mathbf{x}, t_n) = \exp\left(\int_{t_{n-1}}^{t_n} \left[\mu_\Phi(\tau) - \lambda_\Phi(\tau) \right] \, d\tau \right) \phi_{-1}(\mathbf{x}, t_{n-1}). \tag{A.17}$$

This solution suggests the following relation between the coefficients

$$\exp\left(\int_{t_{n-1}}^{t_n}[\mu_\Phi(\tau)+\lambda_\Phi(\tau)]\ d\tau\right)\ \exp\left(\int_{t_{n-1}}^{t_n}[\mu_\Phi(\tau)-\lambda_\Phi(\tau)]\ d\tau\right)$$

$$= \exp\left(\int_{t_{n-1}}^{t_n} 2\mu_\Phi(\tau)\ d\tau\right) = \left[\exp\left(\int_{t_{n-1}}^{t_n}\mu_\Phi(\tau)\ d\tau\right)\right]^2. \tag{A.18}$$

This immediately suggests us to propose the third normalization equation (2.10) to determine the projection parameters. In fact, equation (2.10) can be also obtained from the relation between the chemical potentials in (1.23) by physical intuitions.

Appendix B Derivation of the projection parameters in (2.11)-(2.12)

Summing (2.11) and (2.12), we get

$$2(\sigma_1^n)^2\|\phi_1(\cdot,t_n^-)\|^2 = 1+M-(\sigma_0^n)^2\|\phi_0(\cdot,t_n^-)\|^2. \tag{B.1}$$

This immediately implies

$$\sigma_1^n = \frac{\sqrt{1+M-(\sigma_0^n)^2\|\phi_0(\cdot,t_n^-)\|^2}}{\sqrt{2}\ \|\phi_1(\cdot,t_n^-)\|}. \tag{B.2}$$

Subtracting (2.12) from (2.11), we obtain

$$2(\sigma_{-1}^n)^2\|\phi_{-1}(\cdot,t_n^-)\|^2 = 1-M-(\sigma_0^n)^2\|\phi_0(\cdot,t_n^-)\|^2. \tag{B.3}$$

Again, this immediately implies

$$\sigma_{-1}^n = \frac{\sqrt{1-M-(\sigma_0^n)^2\|\phi_0(\cdot,t_n^-)\|^2}}{\sqrt{2}\ \|\phi_{-1}(\cdot,t_n^-)\|}. \tag{B.4}$$

Multiplying (B.2) and (B.4) and noticing (2.10), we get

$$\begin{aligned}&\left[1+M-(\sigma_0^n)^2\|\phi_0(\cdot,t_n^-)\|^2\right]\left[1-M-(\sigma_0^n)^2\|\phi_0(\cdot,t_n^-)\|^2\right]\\ &= 4\|\phi_{-1}(\cdot,t_n^-)\|^2\ \|\phi_1(\cdot,t_n^-)\|^2\ (\sigma_0^n)^4.\end{aligned} \tag{B.5}$$

Simplifying the above equation, we obtain

$$\begin{aligned}&\left[\|\phi_0(\cdot,t_n^-)\|^4-4\|\phi_{-1}(\cdot,t_n^-)\|^2\ \|\phi_1(\cdot,t_n^-)\|^2\right](\sigma_0^n)^4-2\|\phi_0(\cdot,t_n^-)\|^2\ (\sigma_0^n)^2\\ &+(1-M^2)=0.\end{aligned} \tag{B.6}$$

Solving the above equation and noticing $(\sigma_0^n)^2\ \|\phi_0(\cdot,t_n^-)\|^2 \le (1-M^2)$, we get

$$\begin{aligned}(\sigma_0^n)^2 &= \frac{\|\phi_0(\cdot,t_n^-)\|^2-\sqrt{4(1-M^2)\|\phi_1(\cdot,t_n^-)\|^2\|\phi_{-1}(\cdot,t_n^-)\|^2+M^2\|\phi_0(\cdot,t_n^-)\|^4}}{\|\phi_0(\cdot,t_n^-)\|^4-4\|\phi_{-1}(\cdot,t_n^-)\|^2\ \|\phi_1(\cdot,t_n^-)\|^2}\\ &= \frac{1-M^2}{\|\phi_0(\cdot,t_n^-)\|^2+\sqrt{4(1-M^2)\|\phi_1(\cdot,t_n^-)\|^2\|\phi_{-1}(\cdot,t_n^-)\|^2+M^2\|\phi_0(\cdot,t_n^-)\|^4}}.\end{aligned} \tag{B.7}$$

Thus immediately implies the solution in (2.11).

Appendix C Computing the chemical potentials μ and λ

After we get the ground state Φ numerically, the energy of the ground state can be computed from the discretization of (1.14) immediately. In order to compute the chemical potentials numerically, different formulations can be applied. Here we propose one of the most reliable way to compute them. Multiplying both sides of (1.18) by $\bar{\phi}_1$ and integrate over $\mathbb{R}^d$, we get

$$(\mu+\lambda)\|\phi_1\|^2 = \int_{\mathbb{R}^d} \bar{\phi}_1\ H_1\phi_1\ d\mathbf{x} := (\phi_1, H_1\phi_1). \tag{C.1}$$

Similarly, take the same procedure to (1.19) and (1.20) by multiplying $\bar{\phi}_0$ and $\bar{\phi}_{-1}$, respectively, we obtain

$$\mu\|\phi_0\|^2 = \int_{\mathbb{R}^d} \bar{\phi}_0\ H_0\phi_0\ d\mathbf{x} := (\phi_0, H_0\phi_0), \tag{C.2}$$

$$(\mu-\lambda)\|\phi_{-1}\|^2 = \int_{\mathbb{R}^d} \bar{\phi}_{-1}\ H_{-1}\phi_{-1}\ d\mathbf{x} := (\phi_{-1}, H_{-1}\phi_{-1}). \tag{C.3}$$

Summing (C.1), (C.2) and (C.3), noticing that the ground state Φ satisfying the constraints (1.16), we get

$$\mu + M\ \lambda = (\phi_1, H_1\phi_1) + (\phi_0, H_0\phi_0) + (\phi_{-1}, H_{-1}\phi_{-1}). \tag{C.4}$$

Subtracting (C.3) from (C.1), we get

$$M\ \mu + \left(\|\phi_1\|^2 + \|\phi_{-1}\|^2\right)\lambda = (\phi_1, H_1\phi_1) - (\phi_{-1}, H_{-1}\phi_{-1}). \tag{C.5}$$

Solving the linear system (C.4) and (C.5) for the chemical potentials μ and λ as unknowns and integrating by parts to the right hand sides, we have

$$\mu = \frac{\left(\|\phi_1\|^2 + \|\phi_{-1}\|^2\right) D(\Phi) - M\ F(\Phi)}{\|\phi_1\|^2 + \|\phi_{-1}\|^2 - M^2}, \qquad \lambda = \frac{F(\Phi) - M\ D(\Phi)}{\|\phi_1\|^2 + \|\phi_{-1}\|^2 - M^2}, \tag{C.6}$$

where

$$\begin{aligned} D(\Phi) = \int_{\mathbb{R}^d} \Bigg\{ & \sum_{l=-1}^{1} \left(\frac{1}{2}|\nabla\phi_l|^2 + V(\mathbf{x})|\phi_l|^2 \right) + 2(\beta_n - \beta_s)|\phi_1|^2|\phi_{-1}|^2 + \beta_n|\phi_0|^4 \\ & + (\beta_n + \beta_s)\Big[|\phi_1|^4 + |\phi_{-1}|^4 + 2|\phi_0|^2 \left(|\phi_1|^2 + |\phi_{-1}|^2\right) \Big] \\ & + 2\beta_s \left(\bar{\phi}_{-1}\phi_0^2\bar{\phi}_1 + \phi_{-1}\bar{\phi}_0^2\phi_1 \right) \Bigg\}\, d\mathbf{x}, \end{aligned} \tag{C.7}$$

$$\begin{aligned} F(\Phi) = \int_{\mathbb{R}^d} \Bigg\{ & \frac{1}{2}\left(|\nabla\phi_1|^2 - |\nabla\phi_{-1}|^2 \right) + V(\mathbf{x}) \left(|\phi_1|^2 - |\phi_{-1}|^2 \right) \\ & + (\beta_n + \beta_s)\Big[|\phi_1|^4 - |\phi_{-1}|^4 + |\phi_0|^2 \left(|\phi_1|^2 - |\phi_{-1}|^2 \right) \Big] \Bigg\}\, d\mathbf{x}. \end{aligned} \tag{C.8}$$

Thus the chemical potentials μ and λ can be computed numerically from the discretization of (C.6), (C.7) and (C.8).

REFERENCES

[1] A. Aftalion and Q. Du, Vortices in a rotating Bose-Einstein condensate: Critical angular velocities and energy diagrams in the Thomas-Fermi regime, Phys. Rev. A, 64 (2001), Article 063603.
[2] M. H. Anderson, J. R. Ensher, M. R. Matthewa, C. E. Wieman and E. A. Cornell, Observation of Bose-Einstein condensation in a dilute atomic vapor, Science, 269 (1995), pp. 198-201.
[3] W. Bao, Ground states and dynamics of multi-component Bose-Einstein condensates, Multiscale Modeling and Simulation, 2 (2004), pp. 210-236.
[4] W. Bao, I-L Chern and F. Y. Lim, Efficient and spectrally accurate numerical methods for computing ground and first excited states in Bose-Einstein condensates, J. Comput. Phys., 219 (2006), pp. 836-854.
[5] W. Bao and Q. Du, Computing the ground state solution of Bose-Einstein condensates by a normalized gradient flow, SIAM J. Sci. Comput., 25 (2004), pp. 1674-1697.
[6] W. Bao, D. Jaksch and P. A. Markowich, Numerical solution of the Gross-Pitaevskii equation for Bose-Einstein condensation, J. Comput. Phys., 187 (2003), pp. 318-342.
[7] W. Bao, F.Y. Lim and Y. Zhang, Energy and chemical potential asymptotics for the ground state of Bose-Einstein condensates in the semiclassical regime, Bull. Inst. Math., Academia Sinica, 2 (2007), pp. 495-532.
[8] W. Bao and W. Tang, Ground state solution of trapped interacting Bose-Einstein condensate by directly minimizing the energy functional, J. Comput. Phys., 187(2003), pp. 230-254.
[9] W. Bao and H. Wang, A mass and magnetization conservative and energy diminishing numerical method for computing ground state of spin-1 Bose-Einstein condensates, SIAM J. Numer. Anal., to appear.
[10] M. D. Barrett, J. A. Sauer and M. S. Chapman, All-optical formation of an atomic Bose-Einstein condensate, Phys. Rev. Lett., 87 (2001), article 010404.
[11] E. P. Gross, Structure of a quantized vortex in boson systems, Nuovo. Cimento. 20 (1961), pp. 454-477.
[12] C. C. Bradley, C. A. Sackett, J. J. Tollett and R. G. Hulet, Evidence of Bose-Einstein condensation in an atomic gas with attractive interaction, Phys. Rev. Lett., 75 (1995), pp. 1687-1690;
[13] S.-L. Chang, C.-S. Chien and B.W. Jeng, Liapunov-Schmidt reduction and continuation for nonlinear Schrödinger equations, SIAM J. Sci. Comput., 27 (2007), pp. 729-755.
[14] S. M. Chang, W. W. Lin and S. F. Shieh, Gauss-Seidel-type Methods for Energy States of a Multi-Component Bose-Einstein Condensate, J. Comput. Phys., 202 (2005), pp. 367-390.
[15] M. L. Chiofalo, S. Succi and M.P. Tosi, Ground state of trapped interacting Bose-Einstein condensates by an explicit imaginary-time algorithm, Phys. Rev. E, 62 (2000), article 7438.
[16] F. Dalfovo, S. Giorgini, L. P. Pitaevskii and S. Stringari, Theory of Bose-Einstein condensation in trapped gases, Rev. Mod. Phys., 71 (1999), pp. 463-512.
[17] K. B. Davis, M. O. Mewes, M. R. Andrews, N. J. van Druten, D. S. Durfee, D. M. Kurn and W. Ketterle, Bose-Einstein condensation in a gas of sodium atoms, Phys. Rev. Lett., 75 (1995), pp. 3969-3973.
[18] A. Görlitz, T. L. Gustavson, A. E. Leanhardt, E. Löw, A. P. Chikkatur, S. Gupta, S. Inouye, D. E. Pritchard and W. Ketterle, Sodium Bose-Einstein condensates in the $F = 2$ state in a large-volume optical trap, Phys. Rev. Lett., 90 (2003), article 090401.
[19] T. L. Ho, Spinor Bose condensates in optical traps, Phys. Rev. Lett., 81 (1998), pp. 742-745.
[20] C. K. Law, H. Pu and N. P. Bigelow, Quantum spins mixing in spinor Bose-Einstein condensates, Phys. Rev. Lett., 81 (1998) pp. 5257-5261.
[21] H. J. Miesner, D. M. Stamper-Kurn, J. Stenger, S. Inouye, A. P. Chikkatur and W. Ketterle, Observation of metastable states in spinor Bose-Einstein condensates, Phys. Rev. Lett., 82 (1999), pp. 2228-2231.
[22] T. Ohmi and K. Machida, Bose-Einstein condensation with internal degrees of freedom in alkali atom gases, J. Phys. Soc. Jpn., 67 (1998), pp. 1822-1825.
[23] L. P. Pitaevskii, Vortex lines in an imperfect Bose gas, Soviet Phys. JETP 13 (1961), pp. 451-454.
[24] L.P. Pitaevskii and S. Stringari, Bose-Einstein condensation, Clarendon press, 2003.
[25] L. Simon, Asymptotics for a class of nonlinear evolution equations, with applications to geometric problems, Annals of Math., 118(1983), pp. 525-571.
[26] D. M. Stamper-Kurn, M. R. Andrews, A. P. Chikkatur, S. Inouye, H.-J. Miesner, J. Stenger and W. Ketterle, Optical confinement of a Bose-Einstein condensate, Phys. Rev. Lett., 80 (1998), pp. 2027-2030.
[27] D. M. Stamper-Kurn and W. Ketterle, Spinor condensates and light scattering from Bose-Einstein condensates, Proceedings of Les Houches 1999 Summer School (Session LXXII).
[28] J. Stenger, S. Inouye, D. M. Stamper-Kurn, H.-J. Miesner, A. P. Chikkatur and W. Ketterle, Spin domains in ground state Bose-Einstein condensates, Nature, 396 (1998), pp. 345-348.
[29] S. Yi, Ö. E. Müstecaplioğlu, C. P. Sun and L. You, Single-mode approximation in a spinor-1

atomic condensate, Phys. Rev. A, 66 (2002), article 011601.
[30] W. Zhang, S. Yi and L. You, Mean field ground state of a spin-1 condensate in a magnetic field, New J. Phys. 5 (2003), pp. 77-89.
[31] W. Zhang, S. Yi and L. You, Bose-Einstein condensation of trapped interacting spin-1 atoms, Phys. Rev. A, 70 (2004), article 043611.
[32] W. Zhang and L. You, An effective quasi-one-dimensional description of a spin-1 atomic condensate, Phys. Rev. A, 71 (2005), article 025603.

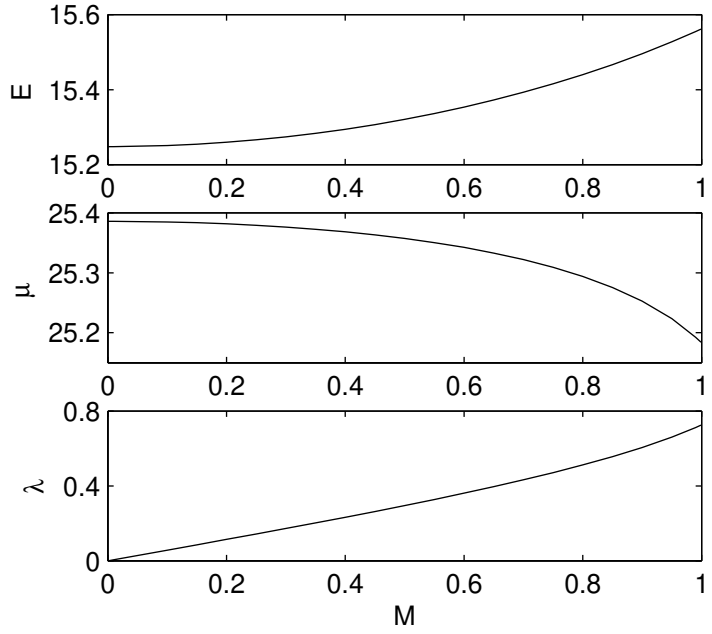
15.6
15.4
15.2
E
0
0.2
0.4
0.6
0.8
1
25.4
25.3
25.2
μ
0
0.2
0.4
0.6
0.8
1
0.8
0.4
0
λ
0
0.2
0.4
0.6
0.8
1
M

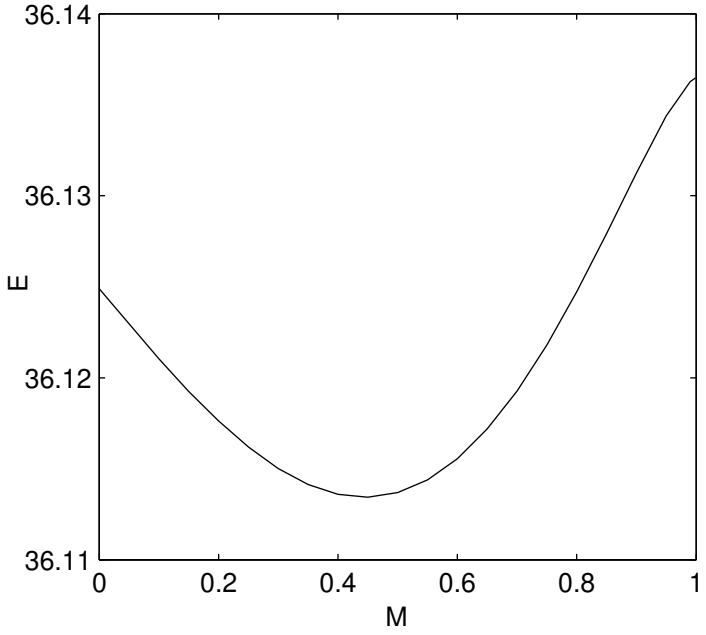
36.14
36.13
36.12
36.11
E
0
0.2
0.4
0.6
0.8
1
M